AIAA JOURNAL
Vol. 47, No. 6, June 2009

# Time-Domain In Situ Characterization of Acoustic Liners in a Flow Duct

K.-Y. Fung*
*The Hong Kong Polytechnic University,*
*Kowloon, Hong Kong Special Administrative Region, People's Republic of China*
X. Jing†
*Beijing University of Aeronautics and Astronautics, 100191 Beijing, People's Republic of China*
and
Z. Lu‡ and X. Yang‡
*The Hong Kong Polytechnic University,*
*Kowloon, Hong Kong Special Administrative Region, People's Republic of China*

DOI: 10.2514/1.36810

**A novel method for measuring liner characteristics in situ in a flow duct is proposed with the immediate aim of obtaining the impedance boundary condition for use in time-domain acoustics. This method as an integrated system in the present demonstration employs an accurate computational aeroacoustics model for prediction of the transient response of a liner to a plane-wave source; an acoustic impulse generator capable of producing sharp, repeatable, millisecond-short sound pulses of desired waveforms; a physical setup of a partially lined duct in a wind tunnel; and an optimization method for parametric identification of the embedded liner. Based on the assumption that impedance can be characterized by a sum of damped harmonic oscillators, the characterizing parameters of the liner are inferred by minimizing the differences between the model-predicted and the in situ measured pressure responses at strategically and conveniently placed sensor locations and are immediate applicable as causal broadband time-domain impedance-equivalent boundary conditions for the computational aeroacoustic model. The use of acoustic impulses of narrow space–time extents affords this method an easy resolve of the influence of neighboring but irrelevant boundaries such as the duct exit. The reliability, effectiveness, and potential benefits of this method are studied and demonstrated. This method is expected to provide broadband inferences and insights into the mean flow effect on liners in a wide range of practical applications with the present setup. It is believed that the feasibility demonstrated here opens a new dimension for theoretical, experimental, and numerical studies in the time domain.**

## Nomenclature

| | | |
|---|---|---|
| $C$ | = | sound speed |
| $d$ | = | orifice diameter of the perforated plate |
| $f$ | = | frequency, Hz |
| $f_x, f_y$ | = | components in the $x$ and $y$ directions of the forcing source $S$ |
| $f_\rho$ | = | volume source component |
| $h$ | = | cavity depth of the microperforated-panel acoustic liner |
| $i$ | = | $\sqrt{-1}$ |
| $L$ | = | characteristic length (grid spacing) |
| $M_x, M_y$ | = | mean flow Mach number components in the $x$ and $y$ directions |
| $p, \hat{p}$ | = | sound pressure and its Fourier-transformed counterpart |
| $\hat{p}^+, \hat{p}^-$ | = | Fourier-transformed incident and reflected sound pressures at a reflective surface |
| $R$ | = | reflection coefficient |
| $S$ | = | forcing source with components $[f_\rho, f_x, f_y]^T$ |
| $t, \Delta t$ | = | time and its increment |
| $u, v$ | = | perturbation velocity components in the $x$ and $y$ directions |
| $\underrightarrow{U}$ | = | solution vector with components $[u, v, p]^T$ |
| $\underrightarrow{w}$ | = | reflection characterizing vector with components $[\mu_n, \bar{\mu}_n, \lambda_n, \bar{\lambda}_n]^T$ |
| $W$ | = | time-domain reflection impulse |
| $(x, y)$ | = | Cartesian coordinates in two dimensions |
| $Z$ | = | acoustic impedance |
| $\delta$ | = | Dirac function |
| $\lambda_k, \mu_k$ | = | complex natural frequencies and amplitudes of the damped harmonic oscillators |
| $\rho_0$ | = | mean air density |
| $\sigma$ | = | open area ratio of the perforated plate |
| $\tau$ | = | thickness of the perforated plate |
| $\omega$ | = | angular frequency |

## I. Introduction

AN ACOUSTIC liner in a duct for noise control and abatement finds numerous applications such as modern ventilation systems, automobile exhaust pipes, and aircraft engines. The design of high-performance silencers requires a clear understanding of the sound-absorbing characteristics of an acoustic liner under various practical conditions. Toward this goal, a great number of methods for measuring duct liner characteristics have been developed over the past decades. Although most efforts have been made on and are continually contributing to frequency-domain techniques, little attention has been paid on time-domain methods. The potential advantages of an acoustic impulse have barely been explored as an effective means to avoid contaminating reflections or to provide broadband phase-accurate information on acoustic systems. Recent advances and interest in computational aeroacoustics (CAA) not only necessitate the extension of the acoustic impedance to its

Presented as Paper 3542 at the 13th AIAA/CEAS Aeroacoustics Conference, Rome, Italy, 21–23 May 2007; received 24 January 2008; accepted for publication 14 February 2009. 

*Professor, Department of Mechanical Engineering, Associate Fellow AIAA.
†School of Jet Propulsion.
‡Research Assistant, Department of Mechanical Engineering.

time-domain-equivalent, but also warrant developments of direct, flexible, measurement technology.

Liner characterization in the presence of a flow has largely relied on the waveguide methods [1–3]. Unlike the popular two-microphone methods [4], these methods allow practicable conditions of a grazing mean flow on partially lined duct walls; do not require intrusive, inconvenient installation of transducers into the liner sample; and can provide global liner-characteristic assessment on practical sample sizes. These methods, as far as we know, have been based on frequency-domain sound-propagation models and have employed harmonic sources for sound-field excitation. They rely on the assumption of a harmonically equilibrium state and theoretically infinite time spans and are therefore susceptible to problems of measurement conducted over practicable finite time periods. A common problem among them is the difficult avoidance of reflections from physical confinements such as the duct ends, which could account for large discrepancies between measured data and CAA predictions [3], and the acoustic characteristics thus educed by matching a CAA prediction with corresponding measured data can hardly guarantee reliable in situ characteristics. The impedance thus measured would be, at best, a dense set of complex values over limited discrete frequencies that may result in algorithmic instability (if directly employed in time-domain CAA methods) or difficult algorithmic implementation (if fitted as a broadband model), due to the subtle causality requirement. The causality of impedance, a key aspect for its time-domain implementation, has neither been considered nor addressed to any meaningful extent in the frequency-domain waveguide methods.

Mindful of these drawbacks, we propose a time-domain method that features the use of short-duration acoustic impulses to excite liner responses. As the reflected impulse would be comparable with the short excitation and have finite space–time extents, the presence of irrelevant boundaries such as the duct exit becomes immaterial for their modeling and prediction, which implies successful system if achieved and thus liner characterization. An acoustic impulse is a rapid rise and recovery of acoustic pressure over a short duration to realize, in practice, the theoretical broadband and frequency-flat delta function. The key to the generation of short-duration pulses is a high level of repeatability and waveform flexibility so that direct and consistent comparison with CAA prediction is meaningful. An advanced impulse-generation technique is adapted and further developed here to produce highly repeatable sound pulses of arbitrary desired waveforms and durations as short as 0.5 ms [5] in a flow-duct or wind-tunnel setting.

A recent advancement in CAA is the advantageous representation of an impedance wall for time-domain applications by a sum of just a few damped harmonic oscillators (DHOs) as structural resonances of the wall or mathematically damped sinusoids. This DHO concept has been benchmarked and validated by accurate prediction of reflections from various termini, including sharp and rounded open ends of a tube [6]. The benchmarked time-domain CAA model [7–9] with liner characteristics implemented as DHOs for prediction of the propagation of harmonic waves and impulses in lined ducts is employed here as the theoretical basis.

Each of the preceding advances is crucial for achieving the proposed time-domain method and is described in detail in the following. Their assembly and realization as a physical system is demonstrated here, together with a study on its reliability, effectiveness, and potential benefits as a novel system for the characterization of liners in situ in a flow. It is believed that the feasibility demonstrated here opens a new dimension for theoretical, experimental, and numerical studies in time-domain acoustics in general and aeroacoustics in particular.

## II. Basic Theory

### A. Implementation of DHO

The reflectivity of an acoustic boundary is conventionally characterized by its impedance or equivalently the reflection coefficient defined for normal incidence as

$$R(\omega) = \frac{\hat{p}^-(\omega)}{\hat{p}^+(\omega)} = \frac{Z(\omega) - 1}{Z(\omega) + 1} \tag{1}$$

which has the time-domain equivalent in the following form of a sum of DHOs:

$$W(t) = \mu_0 \delta(t) + H(t) \sum_k [\mu_k \exp(i\lambda_k t) + \bar{\mu}_k \exp(i\bar{\lambda}_k t)] \tag{2}$$

where $\mu_0$ is real, and both the complex natural frequencies and the corresponding amplitudes appear in pairs as $\lambda_k$ with $\bar{\lambda}_k = \pm\alpha_k + i\beta_k$ and $\mu_k$ with $\bar{\mu}_k = a_k \pm ib_k$, respectively, to ensure that $W$ is a real-valued function. The frequency-domain counterpart of Eq. (2) is

$$R(\omega) = A_0 + \sum_k \frac{iA_k}{\lambda_k - \omega} + \frac{i\bar{A}_k}{\bar{\lambda}_k - \omega} \tag{3}$$

It has recently been established that many common sound-absorbing materials or structures can be effectively characterized over a wide band of frequency by the sum of only a few DHOs [6]. It is therefore advantageous and effective to group these DHO parameters into a reflection characterizing vector $\vec{w} = [\mu_1, \bar{\mu}_1, \lambda_1, \bar{\lambda}_1, \ldots]^T$. The reflected pressure at a boundary point $\vec{x}_b$ can then be computed through the causal Fourier convolution:

$$p^-(\vec{x}_b, t, \vec{w}) = \int_{-\infty}^{t} W(\vec{x}_b, t - \tau, \vec{w}) p^+(\vec{x}_b, \tau) \mathrm{d}\tau \tag{4}$$

Equation (4) can be efficiently implemented by the following two-level recursive time-domain impedance boundary condition (TDIBC) [10]:

$$\begin{cases} p^-(t) = \mu_0 p^+(t) + \sum_k p_k^-(t) \\ p_k^-(t) = \mu_k [p^+(t) + z_k p^+(t - \Delta t)] \frac{\Delta t}{2} + z_k p_k^-(t - \Delta t) \end{cases} \tag{5}$$

where $z_k = \exp(i\lambda_k \Delta t)$. This algorithm is unconditionally stable as $|z_k| < 1$ or $\mathrm{Im}\,\lambda_k > 0$ is required for causal impedance.

### B. Numerical Duct Model

Figure 1 shows the propagation of a sound impulse in a flow duct with partially lined, acoustically conductive walls. The origin of the $x$–$y$ coordinates is taken to be within the plane of the sound source. The governing equation of the propagation and reflection of acoustic waves is the linearized, two-dimensional, inhomogeneous Euler equation:

$$\frac{\partial U}{\partial t} + A_x \frac{\partial U}{\partial x} + A_y \frac{\partial U}{\partial y} = S \tag{6}$$

where

$$A_x = \begin{bmatrix} M_x & 0 & 1 \\ 0 & M_x & 0 \\ 1 & 0 & M_x \end{bmatrix} \quad \text{and} \quad A_y = \begin{bmatrix} M_y & 0 & 0 \\ 0 & M_y & 1 \\ 0 & 1 & M_y \end{bmatrix}$$

The source term $S$ on the right-hand side can accommodate both fluid expansion $f_\rho$ and fluctuating forces $f_x$ and $f_y$, but for the present objective, only the former is retained and modeled as a Gaussian distributed source [8]. For convenience and simplicity, distance, velocity, and time have been nondimensionalized,

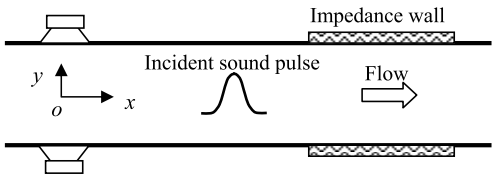


**Fig. 1 Propagation of sound pulse in a duct with partially lined walls.**

respectively, by $L$, $C$, and $L/C$, the dynamic pressure $p$ by $\rho_0 C^2$, and the volume source $f_\rho$ by $\rho_0$.

Following Ju and Fung [9], Eq. (6) is split into two unidirectional sets:

$$\frac{\partial U}{\partial t} + A_x \frac{\partial U}{\partial x} = \frac{S}{2} \quad \text{and} \quad \frac{\partial U}{\partial t} + A_y \frac{\partial U}{\partial y} = \frac{S}{2} \tag{7}$$

each of which is further diagonalized and decoupled (e.g., in the $x$ direction) as

$$\frac{\partial}{\partial t}\begin{bmatrix} v \\ u+p \\ u-p \end{bmatrix} + \begin{bmatrix} M_x & 0 & 0 \\ 0 & M_x+1 & 0 \\ 0 & 0 & M_x-1 \end{bmatrix} \frac{\partial}{\partial x}\begin{bmatrix} v \\ u+p \\ u-p \end{bmatrix} = \frac{1}{2}\begin{bmatrix} 0 \\ f_\rho \\ -f_\rho \end{bmatrix} \tag{8}$$

Thus, Eq. (6) is split into 6 simple unidirectional wave equations, each of which is discretized by the three-point, two-level compact scheme of [7] and closed at both ends of a solution array with the DHO model of Eq. (2) and the TDIBC of Eq. (5). The accuracy of the numerical method has been systematically benchmarked for various linear acoustic phenomena [7–10], among which the transient point-source reflection in free space and the harmonic wave propagation in a lined duct are pertinent to the present study. This 2-D model has also been benchmarked with a comparable, but fully three-dimensional, model.

### C. Identification of DHO

In principle, if a space–time accurate prediction model is available, it should render a forward computation $p_T(\vec{x}, t, \vec{w})$, comparable with the measured pressure $p_M(\vec{x}, t)$ at any suitable location $\vec{x}_m$ within the spatial confinement of the physical model over a finite time span $T$ to a degree of satisfaction measured by the least-squares error,

$$E(\vec{w}) = \int_t^{t+T} [p_M(\vec{x}_m, t) - p_T(\vec{x}_m, t, \vec{w})]^2 \mathrm{d}t \to 0 \tag{9}$$

or in its discrete numerical equivalent,

$$E(\vec{w}) = \sum_{k=1}^{N} [p_M(\vec{x}_m, t_k) - p_T(\vec{x}_m, t_k, \vec{w})]^2 \to 0 \tag{10}$$

over a set of $N$ time-sequence data. Equation (9) or Eq. (10) provides a means for determining $\vec{w}$ that approaches a truthful description of the impedance wall. Theoretically, any finite set of space–time sample data of length $N$ greater than the dimensions of $\vec{w}$ is sufficient to determine the DHO-characterizing parameters $\vec{w}$. Here, we explore the suitability of the Levenberg-Marquardt (L-M) method for a robust optimization algorithm [11].

**Table 1 Specifications of perforated liners**

| Liner | $d$, mm | $\tau$, mm | $\sigma$, % | $h$, mm |
|---|---|---|---|---|
| 1 | 0.35 | 0.14 | 1.07 | 40.0 |
| 2 | 1.0 | 1.0 | 1.21 | 40.0 |

## III. Experiment

### A. Experimental Setup

The schematic in Fig. 2 shows a 2.1-m-long duct, with a $40 \times 40$ mm$^2$ rectangular cross section, mounted between the entrance and exit of a recirculating wind tunnel. The mean flow speed in the duct can be set up to 30 m/s. At the upstream end of the duct is a sound source consisting of two loudspeakers, and at the downstream end are liner samples symmetrically mounted on the top and bottom duct walls. The liners in this study are the resonant type, fabricated of a perforated plate backed by a small-cell-partitioned cavity for locally reacting impedance. Two liners, named liner 1 and liner 2, are chosen for our study here. Their physical specifications are listed in Table 1. Liner 1 has smaller submillimeter pores of larger viscous damping than those of liner 2.

The impulse sound pressure inside the duct is measured by a B&K $\frac{1}{2}$-inch microphone flush-mounted on the duct wall. There are two ports for mounting the microphone: port 1 is 200 mm downstream of the sound source and port 2 is 410 mm ahead of the liners. An NI-DAQ6062E data acquisition board (DAQ) is used for sampling the microphone signal and producing the analog output to drive the loudspeakers. The AI and AO channels of the DAQ board are programmed to be synchronized and have the sampling and updating rates of 100 kHz. A laptop computer equipped with measurement software is used for data acquisition, source control, and data processing.

### B. Impulse Measurement

An advanced impulse-generation technique has been developed that can produce highly repeatable sound pulses of desired arbitrary waveform as short as 0.5 ms [5]. A key to the present impulse measurement is the neutralization of unwanted reflections from either the inlet or outlet of a duct. An active wave-cancellation method, similar to that described in [5], is used to include the effect of the inlet in the generation of a short downstream pulse. Taking the loudspeakers and the upstream inlet in the neighborhood as a whole, we first position the microphone at port 1 to measure the response and the transfer function of the duct-source system with unlined hard

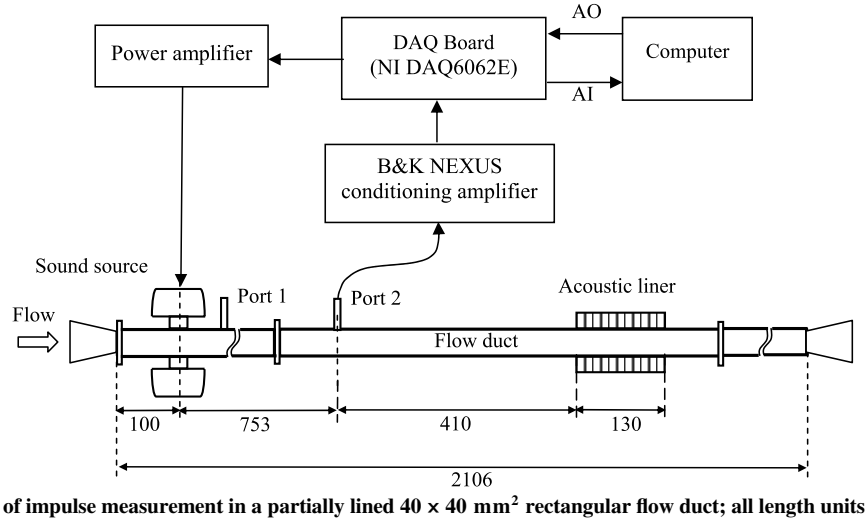


**Fig. 2 Schematic of impulse measurement in a partially lined 40 × 40 mm$^2$ rectangular flow duct; all length units are in millimeters.**

walls and then synthesize the control signal for the loudspeakers to emit only downstream-traveling sound pulses. As the typical impulse duration is about 1 ms long or a span of less than 340 mm, the duct so designed is long enough for editing out the undesired reflections from the downstream duct outlet. Note that the use of short impulses instead of harmonic waves for testing greatly simplifies the experimental setup and makes the employment of anechoic termination unnecessary.

Two types of desired waveforms, referred to as the sine and the three-pole, are used in the present study for cross-checking. The first one is a single-period-sine wave, and the second one is a synthesized signal of three DHOs, or poles, for which the parameters are given in Appendix A of [6], and their durations are approximately 1 ms. Both types of pulses have rounded rise and recovery so that their spatial and temporal resolutions for numerical reproduction are not overly demanding. The spectra of the two pulses are considerably cropped at 4220 Hz in consideration of the present duct size, maximum flow speed, and plane-wave assumption, for which a single flush-mounted microphone is sufficient to measure both incident and reflected impulses. This setup not only greatly simplifies instrumentation and data processing, but also avoids error due to microphone mismatch.

A time-domain averaging method is used to increase the signal-to-noise ratio (SNR), and for the present measurement conditions, the noise level can be effectively reduced (greater than 20 dB signal-to-noise ratios) after averaging 50 times. The measurements reported here were conducted at the room temperature of 19°C or the sound speed of 342.6 m/s.

Figure 3 shows sharp incident pulses of about 1 ms measured at port 2 and various flow speeds. The successive time delays from one pulse to another correspond to the differences in flow speed. At the highest speed, the incident pulse is contaminated by small background noises from the ventilator blades, but the SNR remains high enough for the present purpose of parameter identification. Figure 4 shows the spectra of the incident pulses at $M = 0$.

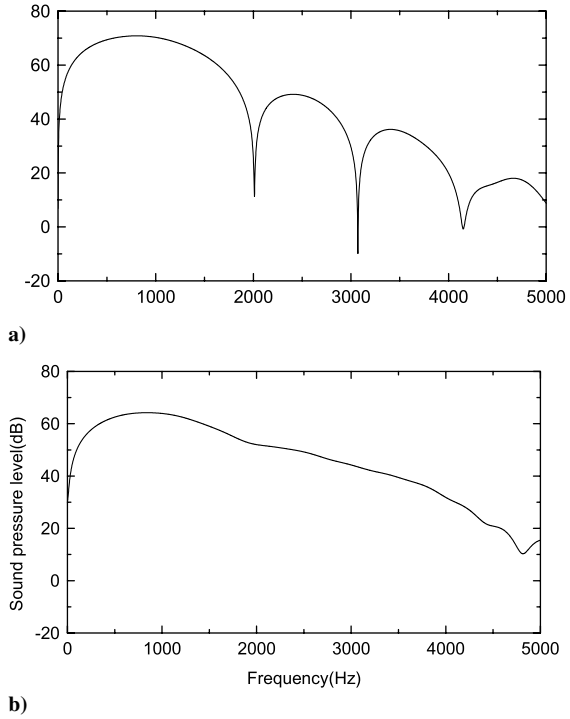


**Fig. 4 Spectrum of the incident sound pulses a) sine and b) three-pole waveform at $M = 0$.**

## IV. Results

### A. Validation of CAA Model

For the present time-domain impedance characterization method, it is imperative that the CAA code be adequately space–time-accurate. We first benchmark the numerical model on the impulse measurements in the simple case of the rigid-walled duct. In the computation, the sound field inside is initialized by two Gaussian distributed sources with a selected half-width of 9.3 grid units, which models the actual acoustic source consisting of two opposite loudspeakers. The actual detail of the source is not important, and the plane wave in the duct is rapidly established within a distance of less than one duct width, due to the restriction on the upper frequencies of the acoustic pulse. When the source strength is set in reference to the

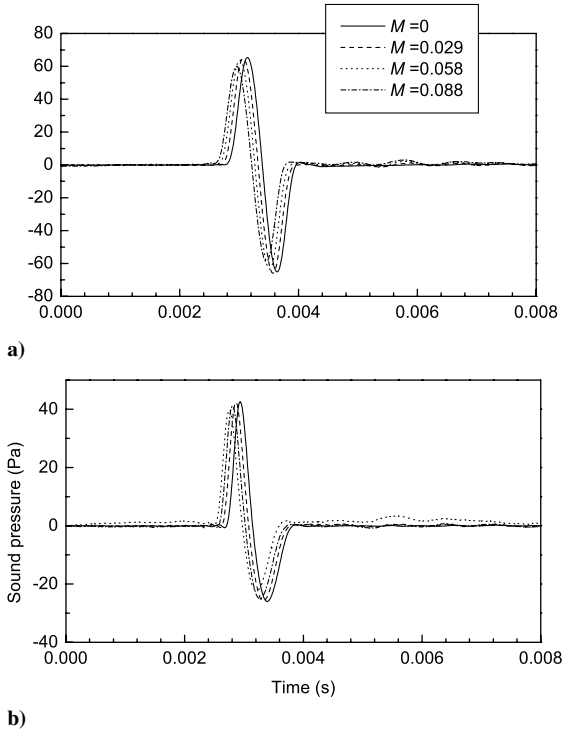


**Fig. 3 Incident sound pulses of a) sine and b) three-pole waveform at various speeds.**

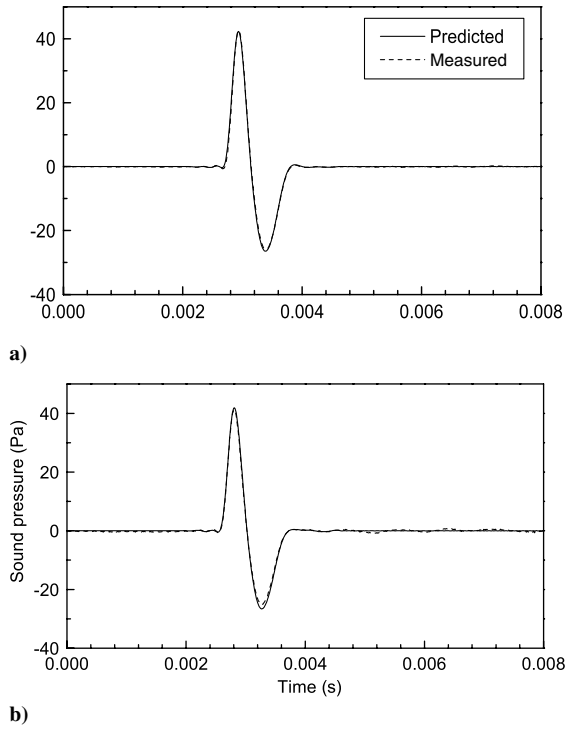


**Fig. 5 Comparison of predicted and measured sound pulses at port 2 for a) $M = 0$ and b) $M = 0.058$.**

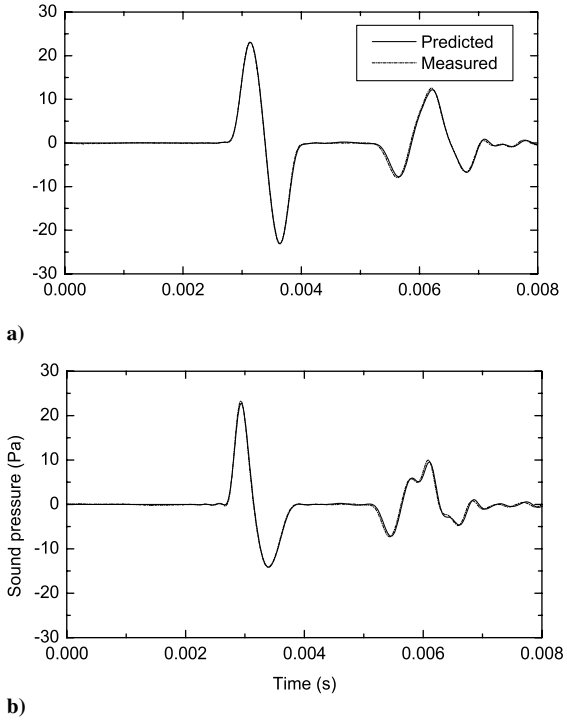


**Fig. 6 Comparison of predicted and measured sound pulses due to the placement of a 40 × 130 × 40 cavity as a liner patch for a) sine and b) three-pole waveform at $M = 0$.**

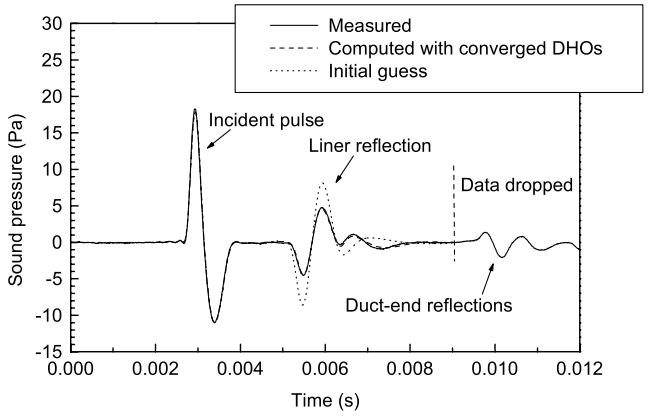


**Fig. 7 Three-pole incident pulse and its trailing reflections, measured and computed, from liner 1 and subsequently from the duct ends at no flow condition, $M = 0$.**

measured pressure at port 1, the predicted incident sound pressure compares well with that measured at port 2 (Fig. 5), confirming the model as a plane-wave guide. Then the $40 \times 130$ mm$^2$ liner patch is covered with a hard-walled 40-mm-deep rectangular cavity. Figure 6 shows a comparison of computed and measured pressures at port 2, confirming the CAA model's validity for the present studies.

### B. DHO Identification

#### *1. Data Truncation and Convergence Criteria*

The solid line in Fig. 7 shows the successive arrivals at port 2 of the three-pole incident pulse and the reflected pulses from the liner and from the downstream duct end for $M = 0$ (no mean flow). It can be seen that the incident pulse is short enough to be clearly separated from the reflected pulse of the acoustic liner. Because of the finite length of the duct, there are also contaminating reflections trailing the liner reflection at a time delay of about 4.4 ms. It should be noted that the duration of the impulse liner reflection is about 4 ms. Therefore, there could be some overlapping between the useful and the

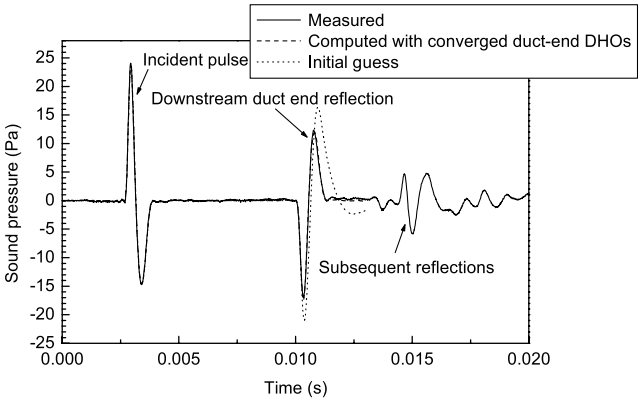


**Fig. 8 Three-pole incident pulse and its trailing reflections, measured and computed, from the duct ends at no flow condition, $M = 0$.**

unwanted signals. An advantage of time-domain methods is that any time sample over a period theoretically contains an infinite amount of information, and a data length $N$ taken over the period with a sufficiently high sampling rate easily exceeds the number of dimensions of the DHO-characterizing vector $\vec{w}$. Here, for the identification of $\vec{w}$, the measured pressure sequence is truncated to not longer than 4.4 ms.

The liners studied here, made of a microperforated plate backed by a cavity, are expected to be represented by only one pair of DHOs [6]. An inverse parametric search begins with the initial estimate of $\mu_0 = 0.5$, $\mu_1 = 0.5$, and $\lambda_1 = 0.5$, which typically gives a largely deviated prediction (dotted line in Fig. 7) from the measured pulse (solid line). As the L-M strategy drives $\vec{w}$ to the target values, the predicted pressure (dashed line) converges to the measured pressure. It is impractical to expect a perfect match between numerically predicted and experimentally measured pressure sequences. The convergence defined by Eq. (10) is set in practice by the normalized bound of squared error in pressure (EP), defined as

$$\mathrm{EP} = \sum_k [p_M(t_k) - p_N(t_k)]^2 \Big/ \sum_k p_M^2(t_k) \tag{11}$$

Typically, about 20 iterations would render an error residue of EP below 1%. Further convergence at higher computing cost is unjustified for the studies here.

If longer data lengths are desired, the reflection from the downstream duct end can be accounted for by first identifying its characterizing vector $\vec{w}$ for the downstream closure without the wall liners. The solid line in Fig. 8 represents the incident pulse (2.6–3.8 ms), the first reflected pulse from the downstream duct end (10.0–11.3 ms), and the subsequent reflections from both ends (beyond 13.9 ms), measured at port 2. The dotted line in Fig. 8 shows the corresponding reflected pulse computed with an estimated DHO vector implemented on the downstream duct end, and the dashed line

**Table 2 Variations of DHO parameters with data length on liner 1**

| Data length | $\mu_0$ | $\mu_k/2\pi$, Hz | $\lambda_k/2\pi$, Hz |
|---|---|---|---|
| | | *Sine pulse* | |
| 4.4 ms | 0.9784 | $-0.7843 - i0.5310$ | $0.9005 + i0.6311$ |
| 3.4 ms | 0.9495 | $-0.7470 - i0.5143$ | $0.8932 + i0.6106$ |
| 2.4 ms | 1.0434 | $-0.9379 - i0.8910$ | $0.7788 + i0.7150$ |
| 1.4 ms | 0.0870 | $-0.9555 - i1.1297$ | $0.6860 + i0.7482$ |
| 1.4 ms | 0.9870 | $-0.9555 - i1.1297$ | $0.6860 + i0.7482$ |
| | | *Three-pole pulse* | |
| 4.4 ms | 1.0282 | $-0.8813 - i0.6603$ | $0.8719 + i0.6785$ |
| 3.4 ms | 1.0292 | $-0.8960 - i0.6996$ | $0.8545 + i0.6881$ |
| 2.4 ms | 1.0756 | $-0.9989 - i1.0064$ | $0.7561 + i0.7355$ |
| 1.4 ms | 0.9956 | $-0.9753 - i1.2953$ | $0.6328 + i0.7428$ |

shows the well-matched computed pulse when the converged $\vec{w}$ minimizes Eq. (11) to the set level.

*2. Data Length and Convergence*

Table 2 lists the converged DHO parameters on various truncated data lengths. Figures 9 and 10 show frequency-dependent reflection coefficients, reconstructed from the listed DHO parameters per Eq. (3), corresponding to the three-pole and the sine incident pulse, respectively. Although it is desirable to use shorter data lengths for DHO characterization, the results in Figs. 9 and 10 suggest that a data length shorter than 3 ms would give substantial deviations from the target. Hence, a data length of 4 ms (400 data points at the present sampling rate) is used for the following DHO analysis.

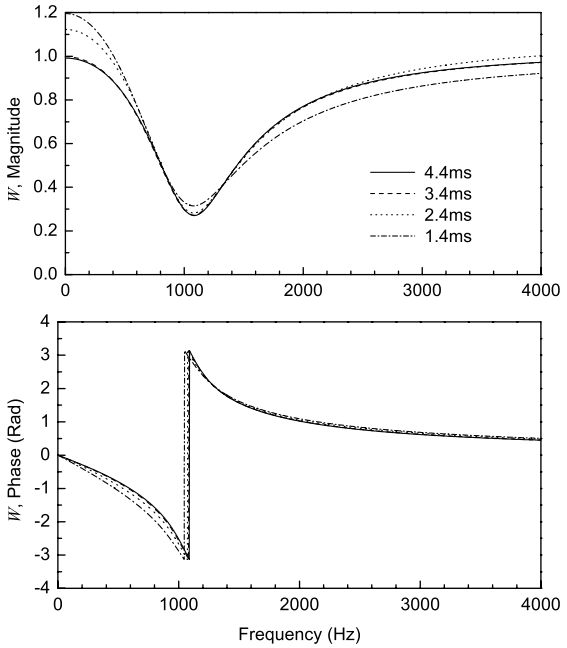


**Fig. 9 Reconstructed reflection coefficients of liner 1 on the three-pole incident pulse and various data lengths.**

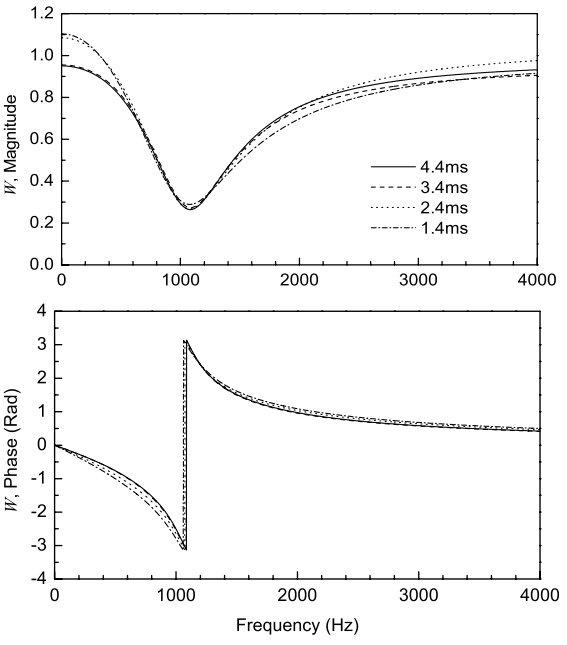


**Fig. 10 Reconstructed reflection coefficients of liner 1 on the sine incident pulse and various data lengths.**

### C. Benchmarking with Impedance-Tube Data

Before applying the present method for in situ impedance characterization under flow conditions, we first benchmark the present results under zero mean flow with those recorded on a B&K 4206 impedance tube. As shown in Figs. 11 and 12, within the frequency range (50–1600 Hz) of the B&K impedance tube, the agreement between the tube-measured and duct-educed reflection coefficients for both liners is quite satisfactory, considering the distinctively different measurement conditions. The impedance-tube method is based on the hypothesis of one-dimensional normal-incident harmonic waves on the impedance sample mounted as the tube terminus, whereas the present method deals with a more complicated situation in which plane-wave pulses graze on liner patches on duct walls with the assumption that the sizable ($130 \times 40$ mm$^2$) liner

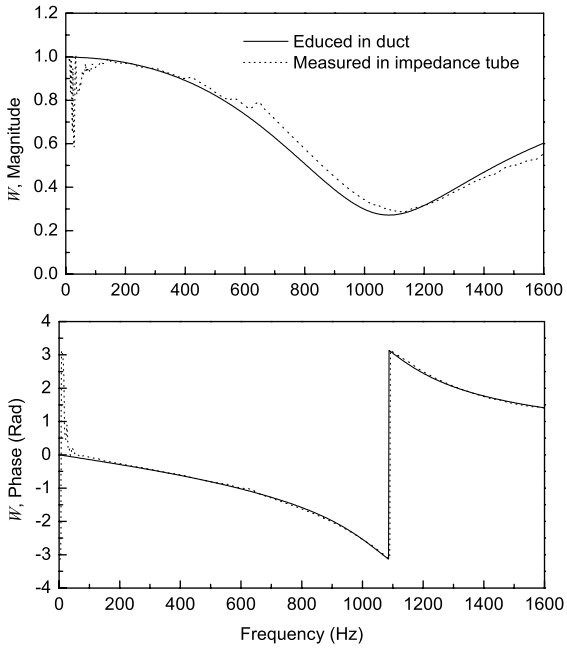


**Fig. 11 Comparison of duct-educed and tube-measured reflection coefficients on liner 1.**

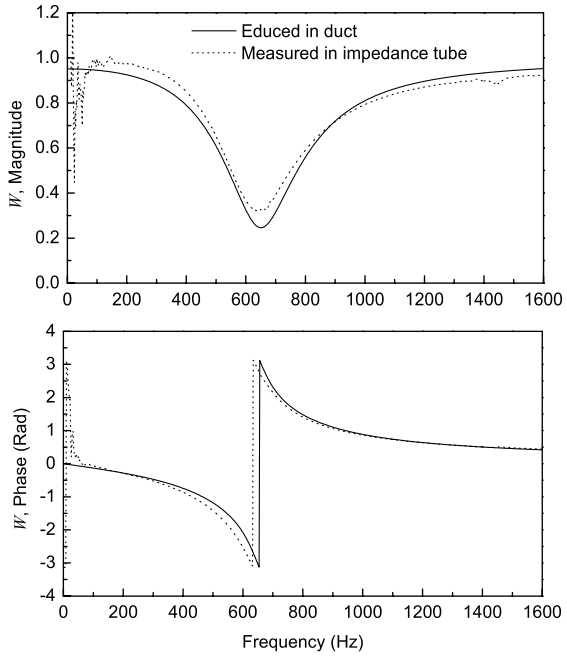


**Fig. 12 Comparison of duct-educed and tube-measured reflection coefficients on liner 2.**

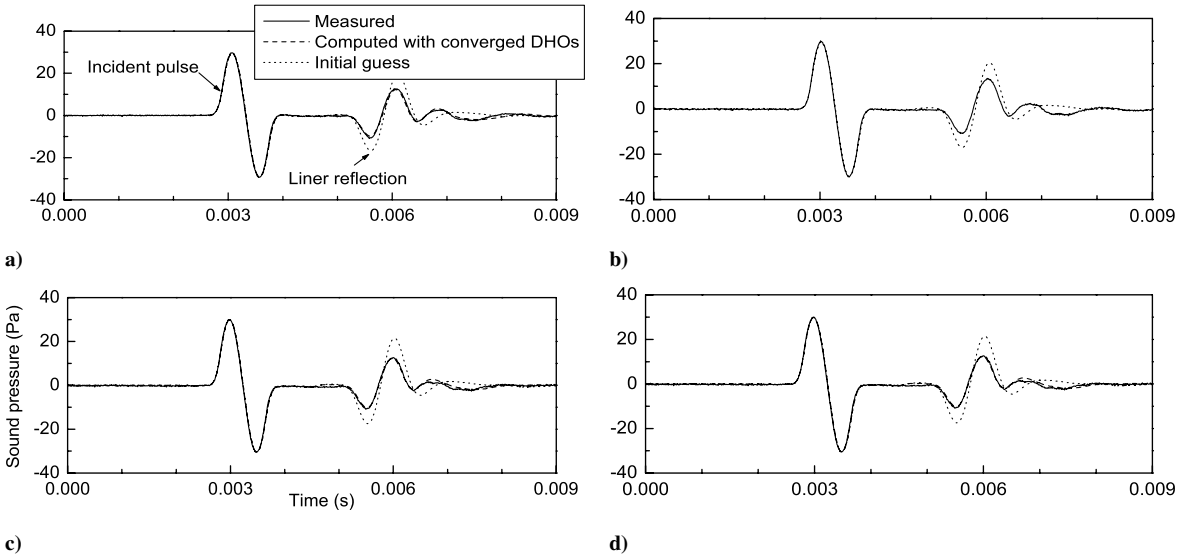


**Fig. 13 Reflections of the sine incident pulse from liner 1 at a) $M = 0$, b) $M = 0.029$, c) $M = 0.058$, and d) $M = 0.088$.**

patches, constructed with a layer of partitioned cavity, are locally reactive with spatially uniform characteristics. In addition, whereas the impedance-tube data are inferred from spatial-equilibrium harmonic waves at discrete frequencies, the present liner characteristics are determined from a direct space–time comparison of measured and predicted wave pulses.

### D. Flow Effects

Figures 13a–13d show reflections of the sine incident pulse from liner 1 at different flow speeds. A single pair of DHOs is assumed for liner characterization with the same initial estimate of $\mu_0 = 0.5$, $\mu_1 = 0.5$, and $\lambda_1 = 0.5$. The initially predicted reflections at different flow speeds (dotted lines in Figs. 13a–13d) deviate largely, but converge after 20 iterations to the dashed lines that are barely discernible from the measured reflections (solid lines), with the EP values of 0.19, 0.22, 1.3, and 0.42% as the corresponding Mach number increases to 0.088 from Figs. 13a–13d. Their educed liner characteristics are shown in Fig. 14 as frequency-varying reflection coefficient $R$ reconstructed from the converged $\vec{w}$. The increased damping effect with flow speed is evident in the progressively-less-pronounced second oscillations in the reflected pulses in Fig. 13 and in the higher resonance frequency with decreased reactance at the phase reversals of $R$ in Fig. 14. These behaviors are also consistent with those of an orifice in a low-speed grazing flow [12]. Figure 15 shows similarly educed reflection coefficients of liner 1 from the reflections of the three-pole incident pulse, cross-checking and clearly substantiating the validity of the present liner characterization method. The identified DHO characteristics $\vec{w}$ for both incident pulses are listed in Table 3, consistently displaying the same flow sensitivities despite some apparent numerical variances. The increasing imaginary part of the complex natural frequency, Im ($\lambda_k$), clearly shows liner 1's increasing resistance characteristic with flow speed.

An obvious source of error, shown in Fig. 13 as deviations between the aft of the incident sine pulse and the front of reflected pulse, is the background noises at higher flow speeds. Although it is

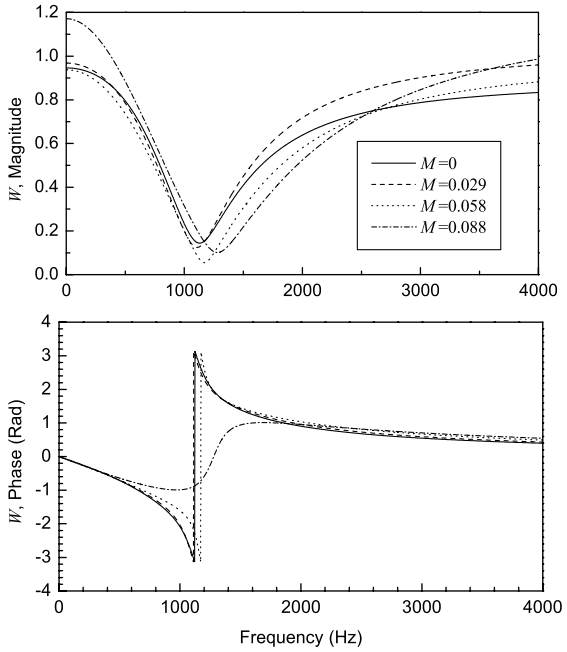


**Fig. 14 Reconstructed reflection coefficients of liner 1 on the sine incident pulse at various flow speeds.**

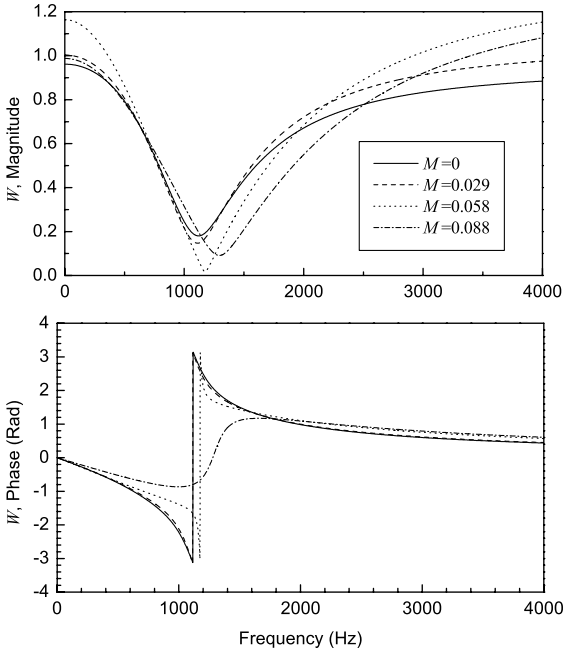


**Fig. 15 Reconstructed reflection coefficients of liner 1 on the three-pole incident pulse at various flow speeds.**

**Table 3 Identified DHO parameters of liner 1 at various flow speeds**

| $M$ number | $\mu_0$ | $\mu_k/2\pi$, Hz | $\lambda_k/2\pi$, Hz |
|---|---|---|---|
| | | *Sine pulse* | |
| 0 | 0.8872 | $-0.6744 - i0.5435$ | $0.8755 + i0.6536$ |
| 0.029 | 1.0281 | $-0.8521 - i0.6776$ | $0.8714 + i0.7390$ |
| 0.058 | 0.9825 | $-0.9483 - i1.0765$ | $0.7752 + i0.9143$ |
| 0.088 | 1.1935 | $-1.3479 - i4.2595$ | $0.3860 + i1.2339$ |
| | | *Three-pole pulse* | |
| 0 | 0.9449 | $-0.7892 - i0.6556$ | $0.8598 + i0.7013$ |
| 0.029 | 1.0498 | $-0.9115 - i0.7859$ | $0.8444 + i0.7615$ |
| 0.058 | 1.3437 | $-1.5480 - i2.9618$ | $0.5463 + i1.1379$ |
| 0.088 | 1.3144 | $-1.6313 - i2.7006$ | $0.6712 + i1.3350$ |

**Table 4 Identified DHO parameters of liner 2 at various flow speeds.**

| $M$ number | $\mu_0$ | $\mu_k/2\pi$, Hz | $\lambda_k/2\pi$, Hz |
|---|---|---|---|
| | | *Sine pulse* | |
| 0 | 0.9877 | $-0.2948 - i0.1258$ | $0.6071 + i0.2521$ |
| 0.029 | 1.0088 | $-0.3097 - i0.1338$ | $0.6219 + i0.2676$ |
| 0.058 | 0.9756 | $-0.3212 - i0.1368$ | $0.6722 + i0.3541$ |
| 0.088 | 0.9147 | $-0.3193 - i0.2494$ | $0.6673 + i0.4518$ |
| | | *Three-pole pulse* | |
| 0 | 0.9874 | $-0.2952 - i0.1215$ | $0.6077 + i0.2455$ |
| 0.029 | 1.0211 | $-0.3178 - i0.1440$ | $0.6139 + i0.2677$ |
| 0.058 | 0.9617 | $-0.3151 - i0.1359$ | $0.6685 + i0.3516$ |
| 0.088 | 0.8265 | $-0.2657 - i0.1609$ | $0.7077 + i0.4223$ |

possible to improve the matches between measured and computed pulses by the employment of more than one pair of DHOs, this was not attempted here, for no drastic change of flow-induced liner characteristics was expected.

The reflections of the sine incident pulse from liner 2 at different flow speeds are shown in Fig. 16, and the effects of flow on the liner characteristics educed from the initial estimate of $\mu_0 = 0.4$, $\mu_1 = 0.4$, and $\lambda_1 = 0.4$ after 20 iterations, within 1% of EP, are shown in Fig. 17. There is also a slight degeneration in the convergence due to increased background noises (Fig. 16), as there is an increased sensitivity to flow damping (Figs. 17 and 18), due to liner 2's larger pores and hence less viscous resistance than those of liner 1 (Fig. 14). The tendency of increasing acoustic resistance with flow speed can also be seen in the identified DHO parameters of liner 2 in Table 4.

## V. Conclusions

An impulse method for acoustic characterization of the partially lined walls of a flow duct has been successfully demonstrated. The use of short impulses limits the space–time extents within a few milliseconds or tenths of meters, which are easily accommodated in most testing facilities and laboratories without the concern of adverse effects from the broader acoustic environment or costly anechoic remedies. This characterization method yields immediately applicable results as TDIBC for CAA applications, as it allows direct assessment of in situ liner performance under practical flow conditions. When there is no mean flow, the present method confirms that the characteristics of a liner in grazing incidence in a duct agree

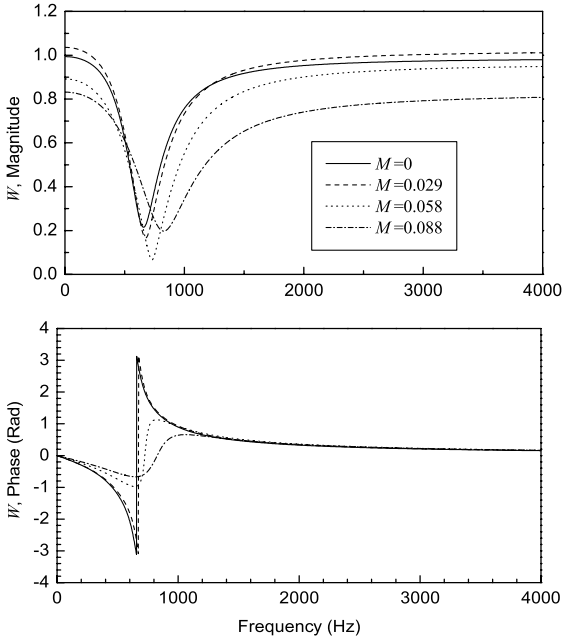


**Fig. 17 Reconstructed reflection coefficients of liner 2 on the sine incident pulse at various flow speeds.**

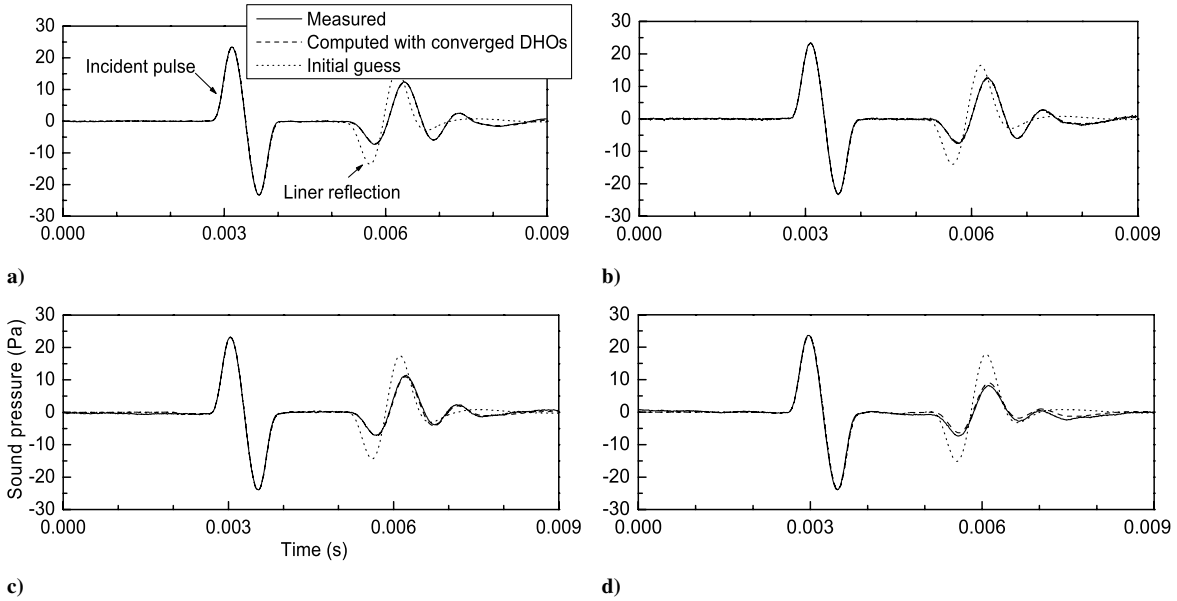


**Fig. 16 Reflections of the sine incident pulse from liner 2 at a) $M = 0$, b) $M = 0.029$, c) $M = 0.058$ and d) $M = 0.088$.**

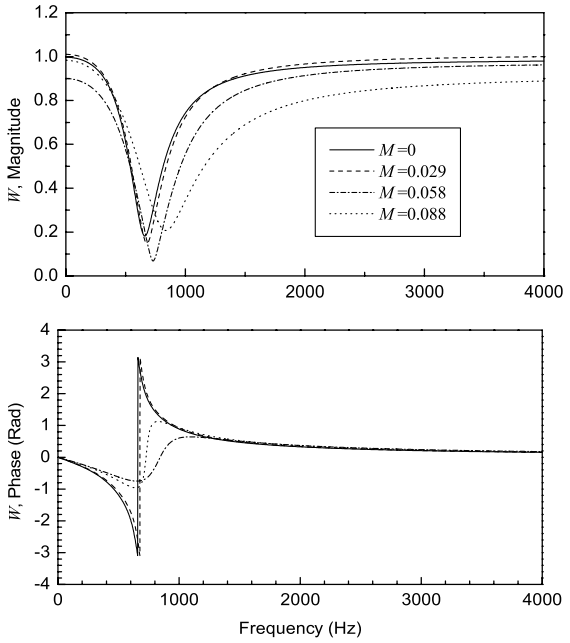


**Fig. 18 Reconstructed reflection coefficients of liner 2 on the three-pole incident pulse at various flow speeds.**

with those of a liner in normal incidence in a reference impedance tube. With the presence of a flow, the method yields sensitive changes in liner characteristics due to the grazing flow. As discernible from the flow-modified reflections, the sensitivity is attributable to the increased liner resistance and decreased reactance as a grazing-flow effect on liner pores.

## Acknowledgments

Financial support for the third and fourth authors from the Hong Kong Research Grants Council's Competitive Earmarked Research grant PolyU 5268/04E and for the second author from The Hong Kong Polytechnic University's Internal Competitive Research grant A-PG67 is gratefully acknowledged.

## References

[1] Jones, M. J., Watson, W., Tracy, M., and Parrott, T., "Comparison of Two Acoustic Waveguide Methods for Determining Liner Impedance," AIAA Paper 2001-2266, 2001.

[2] Elnady, T., Musharraf, M., Bodén, H., and Elhadidi, B., "Validation of an Inverse Analytical Technique to Educe Liner Impedance with Grazing Flow," AIAA Paper 2006-2639, 2006.

[3] Watson, W. R., and Jones, M. G., "Comparison of a Convected Helmholtz and Euler Model for Impedance Eduction in Flow," AIAA Paper 2006-2643, 2006.

[4] Dean, P. D., "An *in situ* method of wall acoustic impedance measurement in flow ducts," *Journal of Sound and Vibration*, Vol. 34, No. 1, 1974, pp. 97–130. doi:10.1016/S0022-460X(74)80357-3

[5] Jing, X., and Fung, K.-Y., "Generation of Desired Sound Impulses," *Journal of Sound and Vibration*, Vol. 297, No. 3-5, 2006, pp. 616–626. doi:10.1016/j.jsv.2006.04.009

[6] Fung, K.-Y., and Jing, X., "Characterization of Impedance Boundary as Damped Harmonic Oscillators via Impulse Reflection," *Journal of the Acoustical Society of America*, Vol. 119, No. 6, 2006, pp. 3831–3837. doi:10.1121/1.2198185

[7] Fung, K.-Y., Man, S. O., and Davis, S., "Implicit High-Order Compact Algorithm for Computational Acoustics," *AIAA Journal*, Vol. 34, No. 10, 1996, pp. 2029–2037. doi:10.2514/3.13349

[8] Ju, H., and Fung, K.-Y., "A Time-Domain Method for Duct Acoustics," *Journal of Sound and Vibration*, Vol. 237, No. 4, 2000, pp. 667–681. doi:10.1006/jsvi.2000.3042

[9] Ju, H., and Fung, K.-Y., "Time-Domain Impedance Boundary Conditions with Mean Flow Effects," *AIAA Journal*, Vol. 39, No. 9, 2001, pp. 1683–1690. doi:10.2514/2.1525

[10] Fung, K.-Y., and Ju, H. B., "Broadband Time-Domain Impedance Models," *AIAA Journal*, Vol. 39, No. 8, 2001, pp. 1449–1454. doi:10.2514/2.1495

[11] Marquardt, D. M., "An Algorithm for Least-Squares Estimation of Nonlinear Parameters," *Journal of the Society for Industrial and Applied Mathematics*, Vol. 11, No. 2, 1963, pp. 431–441. doi:10.1137/0111030

[12] Jing, X., Sun, X., Wu, J., and Meng, K., "Effect of Grazing Flow on the Acoustic Impedance of an Orifice," *AIAA Journal*, Vol. 39, No. 8, 2001, pp. 1478–1484. doi:10.2514/2.1498

R. Ohayon
*Associate Editor*